Impact of initial states on the vapor hydration of iodine-bearing borosilicate glass

Haohan Zhang, Jean-Pierre Guin, Tomo Suzuki-Muresan, Michael Paris, Stéphane Gin, Abdesselam Abdelouas

Impact of initial states on the vapor hydration of iodine-bearing borosilicate glass

Haohan Zhang[a,*], Jean-Pierre Guin[b], Tomo Suzuki-Muresan[a], Michael Paris[c], Stéphane Gin[d], Abdesselam Abdelouas[a]

[a] *SUBATECH, CNRS/IN2P3, IMT Atlantique, Université de Nantes, BP 20722, 44307 Nantes cedex 3, France*

[b] *Institut de Physique de Rennes, Univ Rennes, CNRS IPR-UMR 62051 , F-35000 Rennes, France*

[c] *Université de Nantes, CNRS, Institut des Matériaux Jean Rouxel, IMN, F-44000 Nantes, France*

[d] *CEA, DES, ISEC, DE2D, University of Montpellier, Marcoule, F-30207 Bagnols sur Cèze, France*

Abstract

Under the context of long-term geological disposal of nuclear waste glass, the present work investigates the effect of initial states on the glass chemical durability in the vapor phase and during subsequent leaching. Glass with different finishing steps of polishing and thermal annealing were prepared, vapor-hydrated, and aqueous-altered. Multiple characterizations of mechanical properties and structural modifications were performed to understand the reduction of vapor hydration rates with annealed glasses. Discussions on the degradation of mechanical properties provide insights to understanding the variations of glass chemical durability, which shows a feasible approach to link mechanical and chemical studies together. By looking into the release of boron in the vapor phase, similarities between glass vapor hydration and glass aqueous alteration at residual rate are noticed, which allow the proposition of mechanisms of boron release. Characterizations of the hydrated-then-altered glass reveal the transport-limiting property of the vapor hydrated layer.

Keywords

Borosilicate glass; Vapor hydration; Chemical durability; Mechanical properties

1. Introduction

Hydration of vitrified nuclear glass in the unsaturated vapor phase is considered to be a realistic scenario within the context of nuclear glass long-term disposal. The humid repository environment in the deep geological disposal facilities could make the vapor hydration of nuclear glass an important aging process which would influence the subsequent release of radionuclides confined in the vitrified glass matrix. Various studies have been carried out to investigate the nuclear glass hydration in the unsaturated vapor phase by using the same autoclaves in which relative humidity is controlled by saline solution that is separated from the glass sample by a Teflon holder [1–7]. Different affecting parameters have been evaluated, including temperature, relative humidity (RH), pH (that is controlled by the vapor composition), and glass composition [1–6]. Recent studies draw attention to the effect of initial surface state (roughness, glass stress state) on the glass vapor hydration [7,8]. In the studies of hydration of SON68 glass (French inactive nuclear glass) in the vapor phase, Jegou et al. [8] found a

higher apparent activation energy than the one reported by Bouakkaz, revealing the impact of glass initial states on vapor hydration [9]. The difference in activation energies implies also the difference in the mechanisms of glass vapor hydration which have not been clearly established yet.

In terms of elemental releases during glass vapor hydration, previous studies showed that the vapor hydration of iodine-bearing borosilicate glass (VNaI glass) was accompanied by the partial releases of B, Na, and I in the vapor phase, while the other network formers (Si and Al) were totally retained [7]. The continuous release of boron in the vapor phase makes it possible to trace the glass vapor hydration kinetics by following the boron release. In the studies of borosilicate glass alteration in the aqueous phase, boron is typically used as a tracer of glass dissolution because of its high mobility and low retention in the altered layer [10]. However, a study on the mechanism controlling the residual rate of glass aqueous alteration proposed to reconsider the role of boron as a tracer because the residual rate was found to be controlled by the behavior of boron, which can, in turn, be retained in the alteration layer [11]. In the borosilicate glass structure, boron could be found in either three-coordinated BO_3 or four-coordinated BO_4. As a cross-linking network former, the departure of boron is considered to be responsible for both the creation of nanopores, and the formation of silanol groups which may promote the re-polymerization of the remaining silicate network and thus affects significantly the glass corrosion [12]. Considering the important role of boron during glass aqueous alteration, its behavior may also influence the hydration of glass in the vapor phase. During the alteration of borosilicate glass in the aqueous phase, the transformation from BO_4 to BO_3 via hydrolysis process and the preferential release of BO_3 have been revealed by both solid sample characterizations and simulation works [13–17]. Though the preferential release of three-coordinated BO_3 was also suggested in the study of glass vapor hydration [7], the mechanism of boron release in the vapor phase is still unclear. On the other hand, previous study showed a retention of about 90% iodine in the vapor-hydrated layer [7]. Considering the fact that the vapor-hydrated glass will eventually end up being altered in an aqueous solution, the stability of hydrated glass in contact with aqueous solution should be investigated to have a comprehensive evaluation of the glass chemical durability.

In this study, the surfaces of monoliths of iodine-bearing borosilicate glass (VNaI) are prepared with different finishing steps of polishing and thermal annealing in order to study the effect of what we defined as the “initial sate” on mechanical properties, hydration and alteration kinetics. The so prepared samples are firstly hydrated in the vapor phase, then altered in deionized (DI) water to evaluate their chemical durability. By comparing the behavior of samples in the vapor phase, the impacts of initial states on the glass hydration kinetics is discussed, which bring lights to the rate-limiting mechanisms of glass vapor hydration (especially the mechanisms of boron release). Solid state characterizations are performed to obtain elemental profiles and structural information of the hydrated and altered layers, which suggests a transport-limiting property of the pre-hydrated layer.

2. Materials and Methods

2.1. Sample preparation

The borosilicate glass sample VNaI is provided by CEA (the samples used in the present study are from the same batch used in a previous study [7], with compositions given in **Table A1**, in Supplementary data). Glass monoliths with a dimension of 10mm×5mm×1mm were cut. Glass

monoliths were firstly polished to 3µm by using SiC papers from P800 grade to P4000 grade then with diamond suspension of 3 µm. The polished glass samples were cleaned with acetone, deionized (DI) water, and ethanol in the ultrasonic bath. The samples polished to 3µm are denoted as P-3 type samples. To study the effect of the glass surface initial state on mechanical properties and chemical durability, some of the P-3 samples were further polished by CeO_2 slurry to optical quality (Chemical mechanical polishing (CMP) with CeO_2). After cleaning the glass by the same procedure described above, the sample was annealed at 540 °C for 2h then cooled down slowly to room temperature. The prepared glass samples are denoted as P-3-C-A type samples. To investigate the effect of annealing on glass vapor hydration, a third type of glass surface initial state was prepared by annealing the P-3 samples with the above-mentioned annealing procedure (denoted P-3-A). **Table 1** summarizes the samples considered in this study and the corresponding preparation procedures. P-3, P-3-A, and P-C-3-A represent three initial surface states and define what is called later the pristine state (or pristine glass). The term 'hydrated glass' denotes the glass samples hydrated in the vapor phase, and 'altered glass' for samples altered in the aqueous phase.

Table 1 Summary of glass samples, preparation process, and characterizations

Type	3µm	CeO_2	Anneal	Name	Hydrated	Characterizations/Tests
P-3	Yes	No	No	PG-3-1	No	ToF-SIMS
				PG-3-2	No	AFM/Nano-indentation
				PG-3-3	No	Chemical durability (60 days)
				PG-3-4	No	Chemical durability (2 days)
				VNaI-22	Yes	ToF-SIMS/Chemical durability
				VNaI-24	Yes	---
P-3-C-A	Yes	Yes	Yes	PG-C-A-1	No	ToF-SIMS
				PG-C-A-2	No	AFM/Nano-indentation
				PG-C-A-3	No	Chemical durability (60 days)
				PG-C-A-4	No	Chemical durability (2 days)
				VNaI-31	Yes	TEM//Nano-indentation
				VNaI-32	Yes	---
P-3-A	Yes	No	Yes	VNaI-26	Yes	---
				PG-3-A	No	AFM/Nano-indentation
Powder	---	---	No	PWD-PG	No	NMR
				PWD-H	Yes	NMR

2.2. Chemical durability tests

Chemical durability of pristine glass samples was tested in both vapor phase and aqueous phase. In the vapor phase, hydration tests were performed at 90 °C in a stainless autoclave (same experimental set-up and method as in our previous study is described in [7]). 8 mL of NaCl saline solution (1.75 wt%) was used to control the relative humidity fixed to 99%. The hydration kinetics was followed by applying the physical and chemical methods as detailed in the previous study [7]. The physical method is based on the analysis of glass samples by FTIR Spectroscopy (Bruker-Tensor 27), through which the thickness of hydrated layer could be estimated (as detailed in Supplementary Note 1 in Supplementary data). The chemical method is based on the analysis of saline solution by an inductively coupled plasma mass spectrometry (Quadrupole ICP-MS Xseries 2, Thermoelectron).

In the aqueous phase, the chemical durability was tested by leaching the glass samples in deionized (DI) water at 50 °C in static mode. Alteration tests with two durations were carried out to determine the initial alteration rate and the elemental release behaviors during longer

term. The short-term alteration tests lasted for 2 days with pristine glass samples altered in 15 mL of DI water at 50 °C. Samplings of 0.6 mL of solution were performed after 2, 4, 8, 24 and 48 h of alteration. The longer-term alteration tests lasted for 60 days with pristine glass samples altered in 27 mL of DI water at 50 °C. Samplings of 1 mL of solution were performed after 1, 7, 14, 28 and 60 days of alteration. The initial surface area to solution volume (*SA/V*) ratio is 3.2 m^{-1} and 8.5 m^{-1} for alteration tests of 60 days and 2 days, respectively. The ratios are chosen to avoid important variations in *SA/V* ratios resulting from the samplings and to obtain sufficient elemental concentrations in the leaching solution to facilitate ICP-MS analyses.

The chemical durability of the hydrated VNaI sample was also tested. To verify if there was initial large release of elements at the beginning of the glass aqueous alteration, 4 cycles of rinsing were performed with the hydrated sample. For the rinsing procedure, the hydrated sample was firstly put in 5 mL of deionized water for 1 h at 50 °C; then the hydrated glass was taken out of the first rinsing solution, put in 5 mL of fresh DI water, and altered at 50 °C for another 3 h; the same process was repeated with increased alteration time steps (4 h then 16 h). After the rinsing process, the rinsed sample was altered in 27 mL of DI water at 50 °C. Samplings of 1 mL of solution were performed after 1, 7, 14, 28 and 60 days of alteration.

The collected leaching solution was analyzed by ICP-MS for boron, silicon, and iodine concentration. Boron and silicon were analyzed in HNO_3 with beryllium and scandium as an internal standard. Iodine was analyzed in NH_4OH with indium as an internal standard. The limits of quantification are 0.05 $\mu g \cdot L^{-1}$ for boron, 6.6 $\mu g \cdot L^{-1}$ for silicon, and 0.01 $\mu g \cdot L^{-1}$ for iodine with relative uncertainties of 5 to10%.

The kinetics of glass alteration can be indicated by the normalized mass loss of element *i* (*NL(i)*, g m^{-2}):

$$NL(i) = \frac{C_i}{X_i \times \frac{SA}{V}} \quad (1)$$

with C_i the concentration of element *i* in solution (g m^{-3}), X_i the weight fraction of element *i* in pristine glass, and *SA/V* the ratio of the glass surface area to solution volume (m^{-1}).

From the normalized mass values, it is possible to calculate the equivalent thickness of the altered layer:

$$ET_i = \frac{NL_i}{\rho} \quad (2)$$

with ρ the density of pristine glass (provided in **Table A1**).

2.3. Solid characterization techniques

2.3.1 Atomic force microscopy (AFM) and Instrumented Nano-indentation:

The 3 types of pristine glass samples were investigated for surface roughness, hardness and reduced elastic modulus characterization. The surface roughness of the surfaces was measured by atomic force microscopy (AFM ICON, from Bruker using TAP300Al probes) using tapping™ mode, which was calibrated with silicon atomic steps. For each type of surface preparation, 4 different zones of 5 × 5 μm^2 were imaged. Topographical data were post treated

with Gwyddion software [18] and reported values of roughness (*Rq*) are mean values (and associated standard deviation values) computed over those 4 different zones. Nano-indentation tests were carried out with a nano-indenter testing device (TI-950 from Bruker, with nano-DMA head) equipped with a Berkovich indenter at ambient conditions (21-22 °C, 42-46% relative humidity). The partial unloading (PUL) mode with 20 partial unloading segments on the loading curve and maximum forces (P_{max}) of 1 mN and 9 mN was used for probing the evolution of mechanical properties as a function of depth at the nanometer scale (as shown in **Fig. A2** in Supplementary data). For each (pristine and hydrated) sample at 1 mN (9 mN) indentation maximum load, 150 (50) indents having 20 measurement steps were performed at a constant loading rate for statistic, and at two different randomly chosen areas on the sample. Before that the frame compliance and the contact area (A_c) of the indenter were corrected and calibrated respectively according to the well accepted method described in [19] and using a silica sample that was glued along with the other tested samples of this study with phenyl salicylate onto the stainless-steel plate of the nano-indenter. A_c was calibrated for a 5 to 80 nm contact depth.

The Oliver and Pharr method was applied to determine, from the load-displacement curves, the hardness (H) and the indentation modulus E_r [19]. In the Oliver and Pharr method, the contact depth (h_c) at maximum load is provided by Eq. (3) where h_{max} is the maximal penetration depth measured at maximum load, P_{max}, and the right term of the equation stands for the elastic deformation of the indented surface where ε is a geometrical constant ($\varepsilon = 0.75$) related to the indenter geometry and S is the contact stiffness at unloading defined by Eq. (4):

$$h_c = h_{max} - \varepsilon \frac{P_{max}}{S} \quad (3)$$

$$S = \frac{dP}{dh} = \frac{2}{\sqrt{\pi}} E_r \sqrt{A_c} \quad (4)$$

with h the displacement of indenter.

From h_{max}, P_{max} and S, and knowing $A_c(h_c)$ by calibration, the hardness (H) equals to the mean contact pressure at P_{max} and the indentation reduced modulus (E_r) may be computed by Eqs. (5) & (6) (for diamond indenter, E = 1141 GPa and Poisson's ratio υ = 0.07):

$$H = P_{max} / A_c \quad (5)$$

$$1/E_r = 1/E_{r,\ indenter} + 1/E_{r,\ sample} \quad (6)$$

Note that for partial unloading mode, a value of both H and E_r is computed from each of the 20 partial unloading segments lying between 0 and P_{max}. Due to the large amount of data, post processed indentation measurements were processed using Jupyter notebook environment.

2.3.2 MAS NMR spectroscopy

In order to obtain the glass structural information in the pristine and hydrated glass, ^{11}B, ^{23}Na, and ^{27}Al Solid State Nuclear Magnetic Resonance (NMR) analyses were performed. Glass powder was prepared by crushing and sieving particle sizes between 100 and 125 µm. The glass powder was hydrated during 150 days in a climatic chamber (WEISS WKL64) set at 90 °C and RH at 95%. NMR analyses were carried out with a Bruker Avance III 500 MHz

spectrometer using a 2.5 mm Magic Angle Spinning (MAS) probe. The glass powder was loaded into ZrO_2 rotor with Teflon caps. MAS frequency was set to 30 kHz and recycle delay set to 10 s for ^{11}B and 1 s for ^{23}Na and ^{27}Al. MAS spectra were acquired with a radio frequency field strength of 11 kHz and with a single pulse excitation of π/10 for ^{11}B spectra, π/9 for ^{23}Na spectra, and π/14 for ^{27}Al spectra. The spectra were referenced against $Al(NO_3)_3$ and $NaNO_3$ aqueous solutions and against 1 mol L^{-1} boric acid solution (19.6 ppm) for ^{27}Al and ^{23}Na and 11B, respectively. ^{11}B spectra were firstly processed to remove the probe background and the contribution of satellite transitions to the central band of the spectrum [20,21]. The processed spectra were decomposed by using DMFit2020 freeware [22]. The simplified decomposition method proposed by Jolivet et al. was used to determine the N_4 ratio (fraction of four-coordinated boron over total boron) [21].

2.3.3 Time-of-Flight Secondary Ion Mass Spectroscopy

Glass samples were analyzed by Time-of-Flight Secondary Ion Mass Spectroscopy (ToF-SIMS) for elemental profiling. The profiles of negative secondary ions were obtained by alternating analysis and abrasion cycles. Primary ions of Bi_3^+ were applied for abrasion cycles at 25 keV. The analyzed area was 50×50 μm^2. At the end of the analyses, the depth of the crater was measured by a mechanical profilometer. The sputtering rate was assumed to be constant over time and calculated by dividing the depth of the crater by the total abrasion time. The elemental profiles were then obtained by considering the constant sputtering rate. The analysis was conducted with pristine P-3 and P-3-C-A samples, hydrated VNaI-22 sample, and hydrated-then-altered VNaI-22 sample.

To investigate the passivating property of the altered layer on the hydrated-then-altered VNaI-22 sample, after the first profiling analysis with ToF-SIMS, the sample was immersed during 24 h at room temperature in an ^{18}O labeled water doped with methylene blue (molecule with a 1 nm hydrodynamic diameter). Initial isotopic ratio of $^{18}O/^{16}O$ was 0.86. After 24 h' alteration, the sample traced with ^{18}O and methylene blue was dried by blowing air to remove water adsorbed on the external surfaces, then plunged in liquid N_2 (77 K) for 10 min to freeze the sample (minimize the pore water mobility). The frozen sample was mounted on a cooled sample holder for ToF-SIMS profiling.

3. Results

3.1. Characterization of pristine state samples

3.1.1 Roughness and mechanical properties of pristine state samples

The 3 types of pristine surface states were characterized by AFM for the initial surface roughness (*Rq*) (**Fig. 1**), which gave 5.82 ± 0.12 nm, 5.79 ± 0.37 nm, and 1.46 ± 0.35 nm for P-3, P-3-A, and P-3-C-A samples, respectively. The polishing process with CeO_2 slurry reduced significantly the surface roughness, while the effect of annealing has no noticeable effect on the surface roughness.

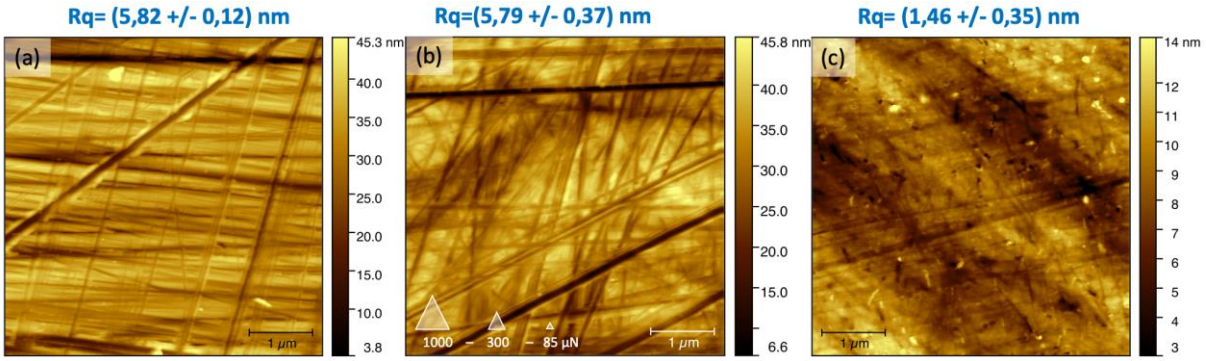

Fig. 1. AFM topography of the VNaI glass surfaces as a function of surface preparation: (a) polished with a 3µm sized diamond suspension (P-3); (b) same as (a) with a subsequent thermal annealing at T_g for 2 h (P-3-A); (c) chemical-mechanical polished with CeO_2, and annealed at T_g for 2 h (P-3-C-A). On figure (b), triangles illustrate the equivalent size of the indentation imprint at h_{max} for loads equal to 1000, 300 and 85 µN. Roughness values were averaged over 4 different areas of 5x5 μm^2 for each sample.

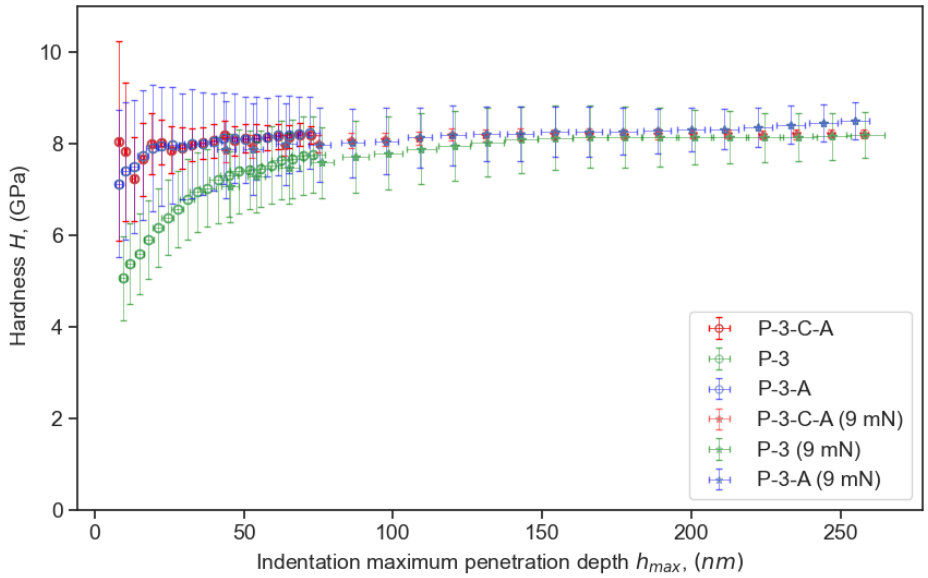

Fig. 2. Evolution of hardness as a function of penetration depth measured by instrumented Berkovich indentation test using a partial unloading set up (20 segments) with maximum loads of 1 mN and 9 mN made on P-3, P-3-A, and P-3-C-A samples. For the 1 mN maximum load data set two areas were tested with 150 indentations imprint each; for 9 mN 50 to 60 indentations were made. Data points represent the mean value of *H* from each unloading segment (at a constant load *P*) at the corresponding mean indentation depth both plotted along with the error bars (± 1 Standard deviation).

The hardness *H* and the reduced modulus E_r of the 3 types of pristine glass samples were determined by instrumented nano-indentation as a function of maximum penetration depth (h_{max}) into the surface. Regarding the elastic property ($E_{r,sample}$, shown in **Fig. A3** in Supplementary data), the surface preparation has no detectable effect on its value, without any differences being largely within the error bars (± 1 standard deviation) from 20 nm up to more than 250 nm for h_{max}. For depth values below 20 nm, a slight difference of few GPa is noticeable between the unannealed sample P-3 and the annealed ones (the shallower the depth, the larger the difference). For hardness (**Fig. 2**), the trend is different: P-3-C-A and P-3-

A exhibit the same behavior on the whole range of tested penetration depth, while P-3 presents a rather different one. From more than 250 nm down to 150 nm, $H_{P\text{-}3}$ has the same and constant value (H = 8.2 ± 0.6 GPa) as the ones measured for P-3-A and P-3-C-A samples. For smaller penetration depths and as penetration depth decreases, $H_{P\text{-}3}$ deviates from the constant H values measured for the 2 other samples and decreases in a non-linear way down to 4.9 ± 0.9 GPa (40% decrease). It is also worth noting that the variability of both H and E_r measurements on P-3-C-A sample is much lower than the one of P-3 and P-3-A samples, it is certainly a direct effect of a lower surface roughness for P-3-C-A when compared to the two others.

3.1.2 Elemental profiles of pristine state samples

To characterize the surface of the pristine glass chemically disturbed by the preparation process, the pristine P-3 and P-3-C-A samples were analyzed by ToF-SIMS. **Fig. 3** gives the profiles of H, B, Na, Al, and I, normalized firstly to the intensity of Siin the disturbed zone then to the intensity ratio with Si in the pristine glass (PG) (Eq. (7)).

$$\text{Normalized intensity of element i} = \frac{\text{Intensity of element i} / \text{Intensity of Si}}{\left(\text{Intensity of element i} / \text{Intensity of Si}\right)_{PG}} \quad (7)$$

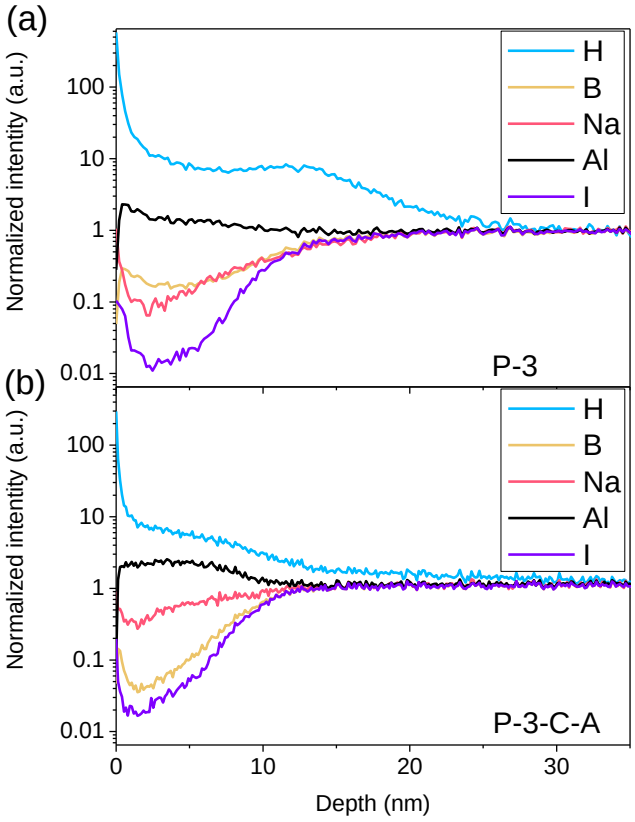

Fig. 3. ToF-SIMS profiles of pristine (a) PG-3-1, the glass sample polished to 3 µm (type P-3) and (b) PG-C-A-1, the glass sample polished to 3 µm and with CeO_2 slurry then annealed (type P-3-C-A).

Si is chosen as the reference for normalization because of its high concentration in VNaI glass. For both samples, it can be seen from **Fig. 3** that the first 20-30 nm (estimation mainly based on the depth of H penetration, from a mechanical viewpoint) of the surface has been altered, which is characterized by a depletion in B, Na and I, and an enrichment in H. This pre-altered layer is usually referred to the Beilby layer formed during the sample polishing [23]. By looking at the profiles of different elements, the estimation of the Beilby layer (or the pre-altered layer) thickness could give different values. In the studies of glass vapor hydration, the commonly used altered layer thickness estimation method considers the thickness to be the depth at which the concentration of B is half of its concentration in the pristine glass [5,7]. The Beilby layer thickness based on boron profiles is about 11.4 nm for polished-only PG-3-1 sample and about 9.2 nm for polished-then-annealed PG-C-A-1 sample. Considering the 10% error for the estimated thickness by ToF-SIMS [24,25], the thicknesses of the Beilby layer are similar between the two analyzed samples. The profiles of H show a larger depth of water penetration in the polished-only sample than in the annealed sample. Besides, within the thicknesses of the Beilby layers (11.4 nm and 9.2 nm, respectively), it could be calculated that about 75% of B, 76% of Na, and 90% of I are lost from the outmost surface of P-3 sample (PG-3-1), while 84% of B, 41% of Na, and 90% of I from the annealed P-3-C-A sample (PG-C-A-1). On the other hand, the recovery of Na can be observed after sample annealing by comparing the profiles of B and Na between P-3 and P-3-C-A samples.

3.2. Chemical durability of glass in the vapor phase and in the aqueous phase

Fig. 4a shows the variations of vapor hydrated layer thickness estimated by FTIR measurements and by the analysis of boron concentration in saline solution. As a general observation, a good repeatability could be found between samples of the same initial surface state. Vapor hydration rate can be estimated through the increase of hydrated layer thickness. An initial hydration rate is calculated by considering the increase of hydrated layer thickness from the beginning of the tests (t = 0 day) to the first FTIR measurement. A reduced initial hydration rate is calculated between the first FTIR measurement and the end of the experiment. **Fig. 4b** gives the vapor hydration rates for the tested samples. For both initial and reduced rates, the polished-only P-3 samples showed significantly larger hydration rate than the annealed P-3-C-A and P-3-A samples.

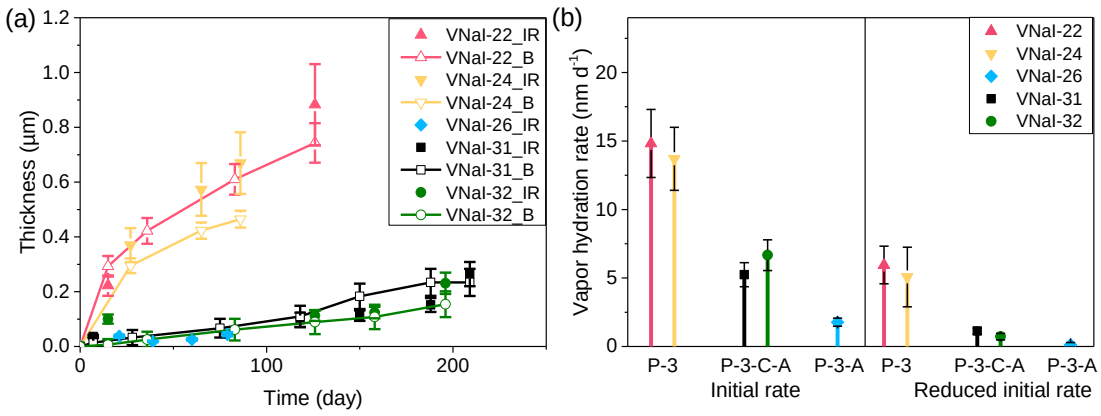

Fig. 4. Vapor hydration kinetics of the 3 types of glass samples: (a) variation of hydrated layer thickness; (b) Initial rate and reduced initial rate. Initial rate is calculated by considering the increase of hydrated layer thickness from the beginning of the tests (t = 0 day) to the first

IR measurement. The reduced initial hydration rate is calculated between the first IR measurement and the end of the experiment.

Fig. 5a, b & c shows the evolution of the alteration layer thickness estimated based on B, I, and Si release from the longer-term (60-day) alteration tests. Similar variations of thickness could be found between P-3 and P-3-C-A samples despite of their difference in initial states. However, for the short-term (2-day) alteration tests (**Fig. 5d**), greater quantity of boron was released from the non-annealed P-3 sample. **Table 2** summarizes the vapor hydration rates (based on FTIR measurements) and the aqueous alteration rates (based on boron release) for the tested samples. The aqueous alteration rates are calculated by dividing the NL_B at 60 days and at 2 days by the total alteration times, respectively.

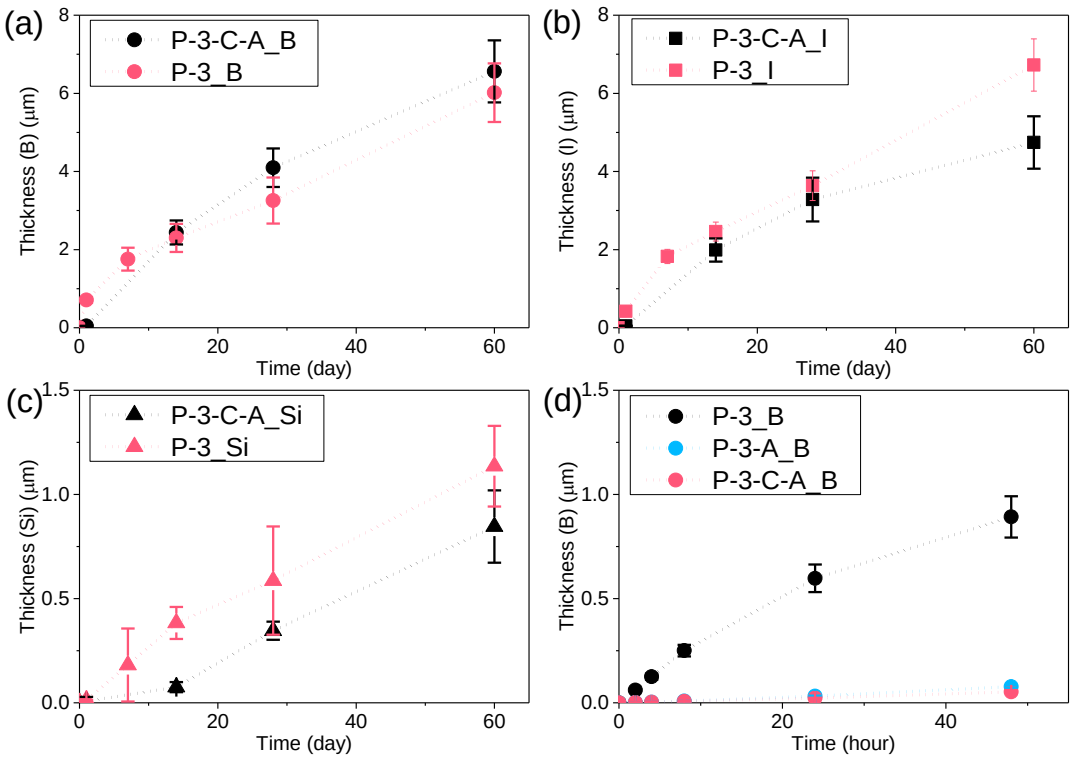

Fig. 5. Data from alteration of pristine glass in DI water at 50 °C. Variation of alteration layer thickness during 60 days of alteration of PG-3-3 (type P-3) and PG-C-A-3 (type P-3-C-A), with thickness estimated based on the release of (a) boron, (b) Iodine, and (c) Silicon. (d) Variation of alteration layer thickness during 2 days of alteration of PG-3-4 (type P-3), PG-3-A (type P-3-A), and PG-C-A-4 (type P-3-C-A), with thickness estimated based on boron release. The initial *SA/V* ratio is 3.2 m^{-1} and 8.5 m^{-1} for the longer-term alteration during 60 days and for the 2-days shorter6-term alteration, respectively.

After 126 days of hydration in the vapor phase, the hydrated VNaI-22 sample was cut into two pieces. One piece of the hydrated sample was used for the characterization of vapor hydrated layer. The other piece was rinsed and altered in DI water for 140 days. **Fig. 6** shows the release of B, I, and Si from the hydrated glass. Comparing the release of elements from the pristine glass and from the hydrated VNaI-22, important reduction in iodine and silicon release is noticed from the hydrated sample, while the release of boron from the hydrated sample is not

affected. The restricted release of iodine and silicon from the hydrated sample indicates a passivating property of the pre-hydrated layer.

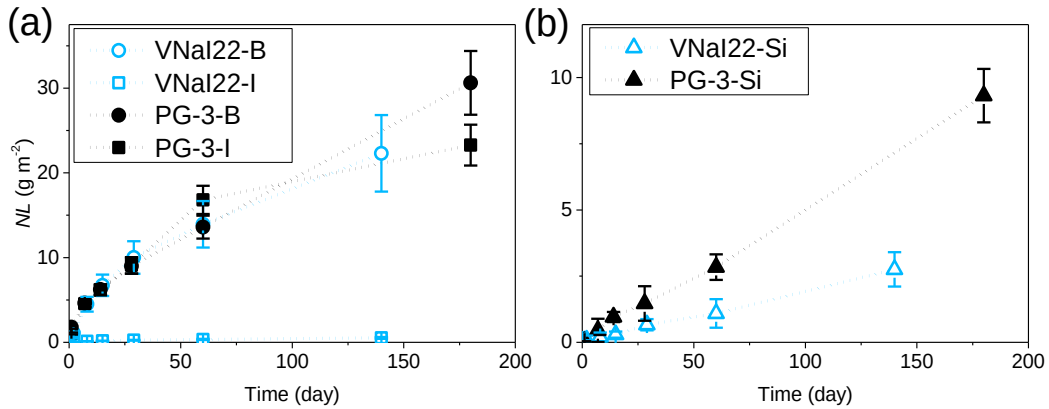

Fig. 6. Data from alteration of hydrated VNaI-22 in DI water at 50 °C. Normalized mass loss of (a) boron and iodine, and (b) silicon from the alteration of pristine glass (PG-3-3, type P-3) and from hydrated VNaI-22.

Table 2 Summary of vapor hydration rates and aqueous alteration rates.

Sample type	Sample name	Initial vapor hydration rate (nm d^{-1})	Reduced initial vapor hydration rate (nm d^{-1})	Short-term aqueous alteration rate (nm d^{-1})	Longer-term aqueous alteration rate (nm d^{-1})
P-3	VNaI-22	14.8 ± 2.5	5.9 ± 1.4	446 ± 50	109 ± 13
	VNaI-24	13.7 ± 2.3	5.1 ± 2.2		
P-3-C-A	VNaI-31	5.2 ± 0.9	1.1 ± 0.2	26 ± 2	100 ± 12
	VNaI-32	6.7 ± 1.1	0.7 ± 0.2		
P-3-A	VNaI-26	1.8 ± 0.3	0.1 ± 0.2	39 ± 3	Non analyzed

Vapor hydration rates are calculated by considering the variation of physical thickness (based on FTIR measurements). Aqueous alteration rates are calculated based on boron release.

3.3. Characterization of hydrated and hydrated-then altered samples

3.3.1 Degradation of mechanical properties of the hydrated layer

After 209 days of hydration in the vapor phase, FTIR spectrum taken on the hydrated VNaI-31 gave a hydrated layer thickness of 264 ± 44 nm (FTIR spectra of hydrated and pristine glass samples are given in Fig. A1 in Supplementary Data). The hydrated VNaI-31 was cut then characterized for hardness and reduced elastic modulus by performing nano-indentation tests at different penetration depths. The hydrated glass samples of type P-3 and P-3-A were not characterized by nano-indentation tests because of the important surface roughness, which would introduce a tremendously large uncertainty on the measurements.

Partial unloading (PUL) instrumented nano-indentation tests allow for exploring the evolution of mechanical properties (H and $E_{r,\ sample}$) as a function of indentation depth. Results are reported in **Fig. 7** and **in Fig. A3** in Supplementary data. For the data sets (P-3-C-A & VNaI-31), matrices of 10x15 indentations with a maximum load of 1 mN were made at two different and randomly chosen areas. 10x10 indentations matrices were also carried on at a third spot location this time with a maximum load of 9 mN. H and $E_{r,\ sample}$ values computed from each

PUL segment of each of the 400 curves (8000 data points in total) are reported in **Fig. 7** and **Fig. A3**, respectively. On **Fig. 7** was also added previous measurements obtained for P-3-C-A and P-3 pristine surface states.

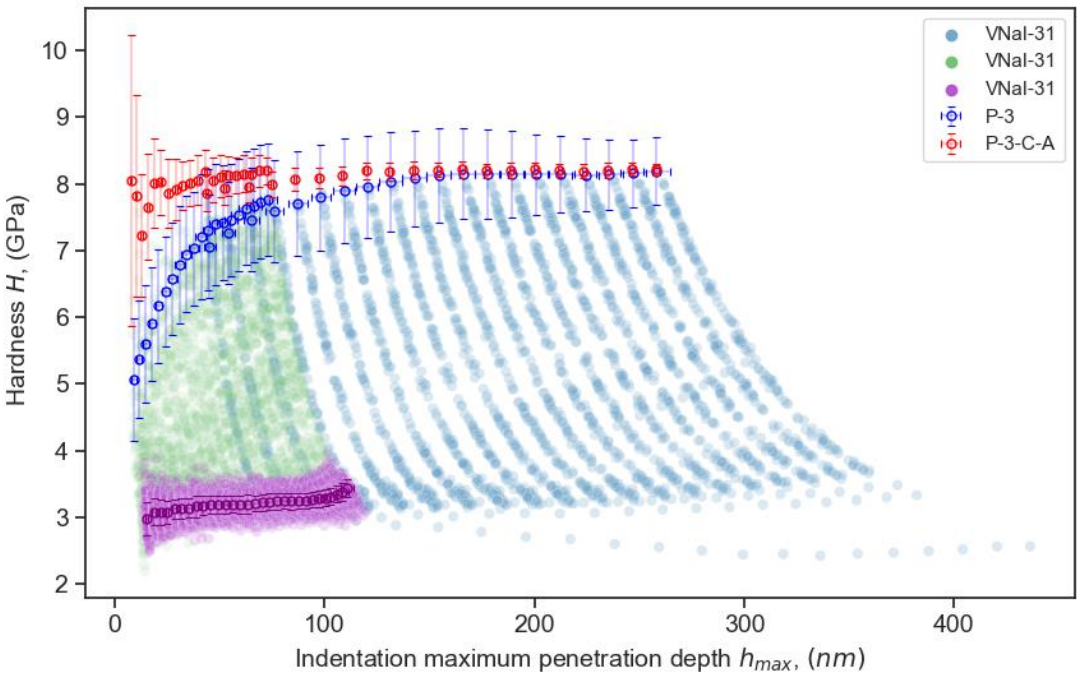

Fig. 7. Evolution of the sample's hardness (H) as a function of penetration depth (h_{max}), at each partial unloading segment (20 segments, P_{max}=1 and 9 mN) performed on P-3-C-A and VNaI-31 samples. While only the mean value and error bars (±1 standard deviation) are reported for P-3-C-A and P-3 pristine state samples, which sets up an upper limit to the possible values of H for the hydrated glass. For the homogeneous area of the VNaI-31 sample (purple points), all the measured values from the data set are reported along with the mean value and error bars computed for each segment (same maximum load). Scattered data points reported in green and in blue stand for different tested areas of VNaI-31 with a maximum load Pmax equal to 1 mN and 9 mN respectively.

The first remark is the large distribution of the data points for each considered depth, which may be understood in terms of heterogeneity of the surface in response to indentation. Nevertheless, this large distribution lies between an upper limit set by the properties of the pristine glass (especially mean values of $H_{P\text{-}3}$ at low penetration depth and a lower limit. The latter is defined from the measurements made at low loads on a quite homogeneous area of the hydrated surface and is illustrated in **Fig.7** by the purple data points for which H does not depend on the indentation depth. This zone is considered to provide the mechanical properties of the hydrated zone of the glass sample (H_{hyd} = 3.2 GPa and $E_{r,hyd}$ = 40.0 GPa).

Following the increase in penetration depth, higher H and $E_{r,sample}$ values are found. Thus, the large scattering of the data points between the upper and lower limit values of H and $E_{r,\,sample}$ reflects the heterogeneity of the hydrated surface in terms of thickness of the hydrated layer. Nonetheless, only few measurements asymptotically reach the hardness of the pristine glass at larger penetration depth (200-300 nm). Regarding $E_{r,sample}$, the same trend is observed (**Fig. A3**), yet not as clear as for H. This is not unexpected as the hydrated sample may be crudely described as a soft and compliant thin hydrated layer on top of a harder and stiffer substrate. As plasticity is more confined around the indenter than elasticity is, E_r is expected to be more

affected (at a shallower indentation depth) by a substrate effect than hardness values. In other words, for very large penetration depth, when compared to the hydrated layer thickness, values of the pristine glass are expected for *H* and $E_{r,sample}$. The plots of *H*- $E_{r,sample}$ provides another way of looking at the data (see **Fig. A5** in Supplementary data), which confirms this behaviour

The inhomogeneity of the surface hydrated layer reported through mechanical properties characterization is compatible with surface observations from TEM-EDX analysis performed on a thin foil extracted from the hydrated surface (**Fig. A6 and A7** in Supplementary data). The later revealed also the inhomogeneity of the hydrated surface of the VNaI-31 sample (**Fig. A6**). Besides, no-significant change in chemical composition was observed (**Fig. A7**).

3.3.2 ^{11}B-NMR of pristine and hydrated glass

MAS NMR spectroscopy was used to characterize the pristine and hydrated glass powder (with initial particle size between 100 and 125 µm). As seen in **Fig. 8**.

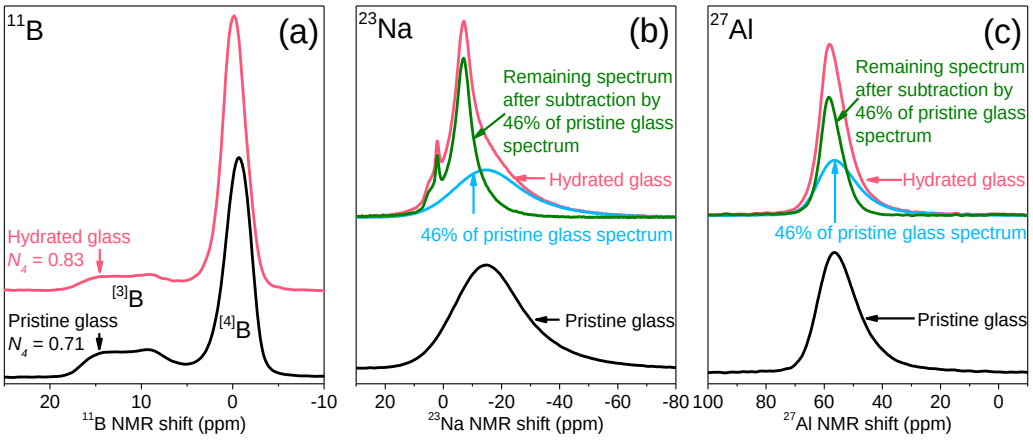

Fig. 8. MAS NMR spectra of pristine and vapor hydrated VNaI glass: (a) ^{11}B spectra of pristine and hydrated glass; (b) ^{23}Na, and (c) ^{27}Al spectra normalized to the surface area, with hydrated glass spectra subtracted by a fraction of the pristine glass spectra.

The ^{27}Al MAS NMR spectrum of the pristine VNaI shows a broad asymmetric resonance due to both distributions of electric field gradient (EFG) and of isotropic chemical shifts. The ^{27}Al MAS NMR spectrum can be fitted by a single line ('Czsimple' model of DMFit freeware) at 62 ppm (δ_{iso}, isotropic chemical shift), C_Q = 4.9 MHz (mean quadrupolar constant) and FWHM(CS) = 11 ppm (full width at half maximum of the Gaussian distribution of isotropic shifts). The spectrum of the hydrated glass shows a slightly narrower resonance, which is due to the presence of neighboring water [26]. Similar reduction of linewidths of ^{27}Al MAS NMR spectra was also observed for glass samples altered in the aqueous phase [26,27]. Spectral decomposition gives δ_{iso} = 62 ppm, C_Q = 4.1 MHz and FWHM(CS) = 7 ppm. Hence, for both pristine and hydrated glass samples, Al only occurs as AlO_4 and no evidence of the presence of AlO_6 is found (expected at ~0 ppm) after alteration.

The ^{23}Na MAS NMR spectrum of the pristine VNaI also shows a broad featureless asymmetric resonance. The ^{23}Na MAS NMR spectrum can be fitted by a single line ('Czsimple' model) at δ_{iso} = -5 ppm with C_Q = 3.0 MHz and FWHM(CS) = 21 ppm. Here again, the ^{23}Na MAS NMR spectrum of the hydrated glass sample exhibits a more symmetrical line shape with reduced

linewidth due to the presence of neighboring water. A new narrow peak is observed at about 2.1 ppm, which may indicate the formation of sodium-containing secondary (possibly crystalline) phases.

^{11}B MAS NMR spectra show narrow and broad resonances for BO_4 ($^{[4]}$B) and BO_3 ($^{[3]}$B), respectively [20,28,29]. The fraction of BO_4 over total boron (N_4 ratio) can be determined rather easily through the area under the MAS peaks. Therefore, the simplified peak decomposition approach proposed by Jolivet et al. was applied [21]. The N_4 ratio is determined to be 0.71 for pristine glass and 0.83 for hydrated glass powder. Though an increase of N_4 ratio from 0.71 to 0.83 is found, it should be noted that the pristine glass could still be present beneath the hydrated layer that covers the external part of the glass particles. As a result, the N_4 ratio of the hydrated layer could be higher than 0.83. The experimental spectra of the partially hydrated glass sample could be considered as the sum of the pristine one and the totally hydrated one. However, the NMR spectra of a totally hydrated sample is unknown in our study. In this case, only a maximum contribution from the pristine glass could be estimated by subtracting the spectrum of the partially hydrated sample by the spectrum of pristine sample while maintaining the positive intensity for the subtracted spectrum. The NMR spectra were firstly normalized to the surface area. With the ^{23}Na NMR spectra, a maximum fraction of 46% is found. Interestingly, the same fraction is obtained with the ^{27}Al spectra. Taking into account the 46% of the pristine glass in the partially hydrated glass sample, the N_4 ratio for the totally hydrated layer is calculated to be 0.93, which indicates the predominance of four-coordinated boron in the hydrated layer.

3.3.3 Elemental profiles of hydrated and hydrated-then-altered P-3 samples

The hydrated VNaI-22 and the hydrated-then-altered VNaI-22 were characterized by ToF-SIMS for elemental profiling in the degraded layers. The profile of hydrated VNaI-22 has been presented in the previous study, showing a hydrated layer of 830 nm with 9% of boron and 92% of iodine retained therein [7]. To further investigate the passivating properties of the hydrated layer, the hydrated-then-altered glass was immersed during 24 h at room temperature in an ^{18}O labeled water doped with methylene blue. The molecules of methylene blue have a hydrodynamic diameter of 1 nm and can be traced by the profile of sulfur. The penetration of methylene blue could imply the presence of pores or channels with diameters larger than 1nm. The change of isotopic ratio of ^{18}O/^{16}O could indicate the fraction of pores accessible to water molecules.

Fig. 9a shows the ToF-SIMS profiles of hydrated-then-altered VNaI-22 glass. The glass sample was firstly hydrated in the vapor phase during 126 days then altered in DI water for 140 days. The elemental profiles in the hydrated-then-altered layer show depletion of boron and sodium and retention of iodine, which are similar to the profiles obtained on the hydrated VNaI-22. Moreover, the great retention of iodine in the hydrated-then-altered layer is not surprising because iodine was merely released during the alteration tests (**Fig. 6**). At about 1300 nm, a local maximum concentration of boron and iodine is observed indicating a possible accumulation of boron and iodine at this depth. Based on the profile of boron, the thickness of the hydrated-then-altered layer is estimated to be 8.3 µm. The NL_B obtained during the alteration of the hydrated VNaI-22 indicates that an altered layer of 8.7 µm has been developed after 140 days of alteration in DI water. However, it should be noted that the surface of the

hydrated-then-altered glass shows a non-negligible roughness, which could induce great uncertainties in estimating the thickness of the degraded layer.

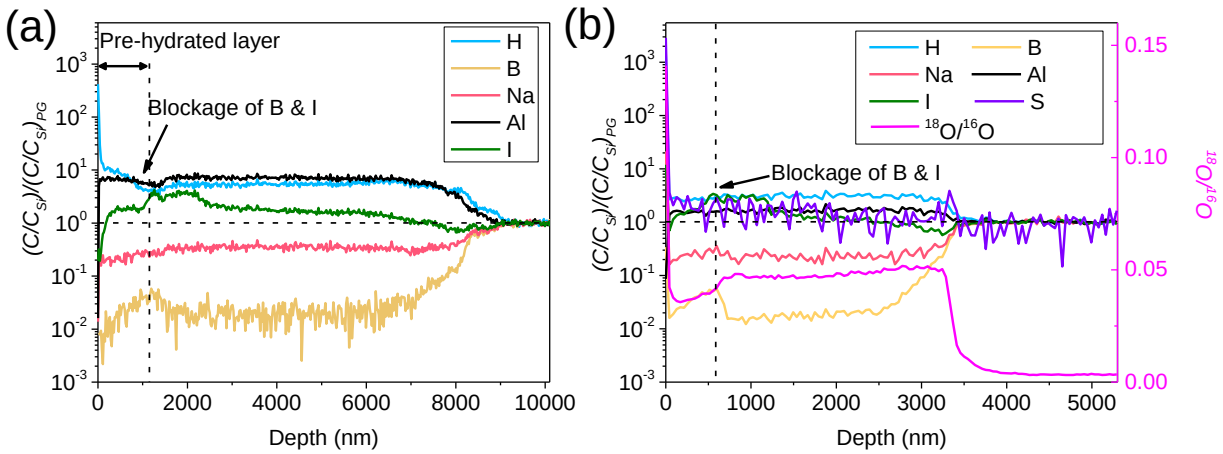

Fig. 9. ToF-SIMS profiles of hydrated-then-altered VNaI glass (a) before and (b) after tracing with ^{18}O and methylene blue.

Fig. 9b gives the ToF-SIMS profiles obtained from the hydrated-then-altered glass sample after tracing with ^{18}O and methylene blue. The blocking barrier of boron and iodine release (implied by the local maximum concentration of the two elements) is located at about 550 nm. The thickness of the hydrated-then-altered layer is about 3.3 µm. The difference in thickness of the hydrated layer (or the depth of the blocking barrier) and of the hydrated-then-altered layer could be due to the inhomogeneity of the degraded surface layer as the elemental profiles are taken at different positions on the glass sample. The profile of methylene blue in the glass sample is marked by the profile of sulfur. It can be seen that the methylene blue molecules did not penetrate into the hydrated layer (or the hydrated-then-altered layer), which indicates that pore sizes of the hydrated layer should be smaller than 1 nm.

By applying the method proposed by Gin et al., the fraction of pores accessible to water molecules can be calculated based on the elemental and isotopic profiles obtained on the hydrated-then-altered layer traced with ^{18}O [25]. By supposing that the pores (assumed to be spherical) in the hydrated-then-altered layer were created by the release of soluble elements (B, Na, and I for the current VNaI sample), the total volume of pores could be calculated based on the elemental profiles. The ionic volumes considered in the calculation are given in **Table A2** in Supplementary data. The co-existence of three-coordinated BO_3 and four-coordinated BO_4 has been considered when calculating the total pore volume, with the N_4 ratio (equals to 0.71) determined by NMR analysis of pristine VNaI glass powder. However, the modification of N_4 ratio in the altered layer was not considered. With the calculated total pore volume in the hydrated-then-altered layer, a hypothetical isotopic ratio of $^{18}O/^{16}O$ could be determined by assuming that all the pores are filled with the ^{18}O labelled water. On the other hand, the ToF-SIMS analysis provided experimental profile of $^{18}O/^{16}O$ in the hydrated-then-altered layer. The isotopic profile was firstly corrected by fixing the isotopic ratio in the pristine glass to the natural abundance of ^{18}O (0.002). The fraction between the corrected isotopic ratio and the hypothetical isotopic ratio could then be considered as ratio of pores that are accessible to water molecules during 24 h of alteration. **Fig. 10** shows the low fraction of accessible pores, about 3-4%, in the first 1800 nm of the hydrated-then-altered layer. It should be noted that the

calculation of the accessible pores fraction considered only the oxygen exchange among water molecules. In the altered layer, oxygen of water molecules may exchange continuously with oxygen atoms from silanols and structural (bridging) oxygen. Nevertheless, the low exchange ratio of oxygen is attributed to the self-reorganization of the altered layer, explaining its passivating property [25]. For the small value of fraction of accessible pores observed in this study, especially within the first 500 nm (corresponding to the vapor-hydrated layer),it suggests also the blocking properties of the hydrated layer in limiting the transport of boron and iodine ions with water molecules.

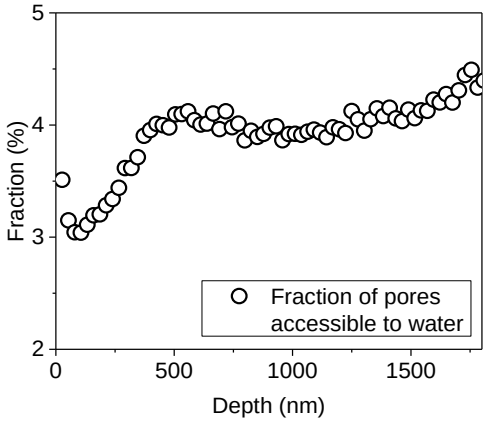

Fig. 10. Fraction of pores accessible to water molecules in the hydrated-then-altered layer.

4. Discussions

4.1 Impacts of polishing and annealing on glass initial states

Characterizations of the pristine glass samples of different initial states (P-3, P-3-A, and P-3-C-A) showed the existence of an outmost layer that is physically and chemically modified by the polishing process and by the subsequent thermal treatment. This modified layer is often referred as the Beilby layer [30,31]. For oxide glasses, this layer results from both the mechanical action of the slurries on the glass surface (densification, microcracks) and the mechanochemical interaction of the slurry with the glass surface which lead to a gentler material's removal. The glass composition, the nature of the slurry as well as the supporting medium (often a liquid) will affect the relative importance of the two above-mentioned mechanisms and the properties of the resulting Beilby layer. Beilby layer is reported to be composed of an outmost hydrated layer followed by a densified layer at deeper depth, thicknesses of which will depend on the polishing parameters such as stress applied, liquid used for polishing, and nature of the particles (diamond, alumina, CeO_2…). Névot and Croce reported a hydrated layer of 1.1 nm and a densified sublayer of several tens of nanometres' thick having a maximum density at a depth of 5.1 nm for chemical mechanical polishing (CMP) conditions with CeO_2 [32]. Using TEM, Toyolo et al. reported that the thickness of the modified layer, depending on polishing conditions, could be up to 150 nm for polished PECVD SiO_2 film deposited onto Si [33]. Further TEM investigations revealed the presence of 2 sub zones in this hydrated layer: the first one, which was chemically altered, extends 3-4 nm below the polished surface, while the second one whose thickness varies between 15 and 20 nm was attributed to a plastically densified region. This structure of layers agrees well with values previously reported using small angle X rays by Nevot and Bensch [32,34]. Therefore, as a rule of thumbs, the main difference between CMP polished glass surface with CeO_2 (P-3-C-A

sample) and diamond polished surfaces (P-3 samples) will be for the later: a larger thickness of the pre-hydrated layer, the presence of a larger and deeper densified layer along with the possible existence of sub surface damages (micro and sub microcracks).

The next point to be discussed is the effect of a high temperature (at transition temperature, T_g) thermal treatment on the Beilby layer. First, it is well established that indentation-induced densification is known to be totally cured by a sub-Tg (0.9*Tg, 2h) thermal treatment leading to no difference in dissolution rate at a previously densified site once thermally cured [35–37]. Moreover, thermal treatment at T_g allows for both the dehydration and the dihydroxylation of oxides glasses [38–40].

Considering the thermal cure of annealed samples, the decrease of hardness values with decreasing penetration depth observed for P-3 sample only is related to the presence of a modified and hydrated layer at the outmost surface. Furthermore, for soda lime and borosilicate glasses, it was shown that the effect of the hydrated layer on the apparent elastic modulus ceased at a penetration depth equal to the thickness of the hydrated layer [41]. From **Fig. A3**, P-3 behavior departs slightly from the one of P-3-A samples within a penetration depth of about 20 nm, which would set an approximate value of this layer thickness. The later value agrees well with the P-3 ToF-SIMS measurements reported in **Fig. 3a**, especially when remembering that water content is known for altering the mechanical properties of glass [42,43] and considering that hydrogen concentration is at a maximum value down to a depth of 15 nm followed by a smooth decrease reaching the bulk glass value at a depth of approximately 25 nm.

4.2 Influence of initial states on glass vapor hydration

Glass samples (P-3-C-A) showed a net decrease in surface roughness after polishing with CeO_2 slurry, while no effect of annealing was observed in modifying the surface roughness (P-3 and P-3-A samples). When comparing the chemical durability in the unsaturated vapor phase and in the aqueous phase (with short-term alteration tests), a major difference was observed between the annealed and the unannealed glass samples. The two types of the annealed samples (P-3-C-A, P-3-A) showed no noticeable difference in hydration kinetics, although a smaller surface roughness was found on the P-3-C-A glass. These observations suggest thus minor effect of surface roughness on the kinetics of glass vapor hydration.

As discussed above (Section **4.1**), the polished P-3 glass may present a larger and deeper densified layer along with the possible existence of subsurface damages (micro and sub microcracks). The plastically densified layer is considered to be formed due to the compressive stress created by contacting with the abrasive particles [44,45]. Molecular dynamics simulation works concerning the chemical mechanical polishing of silicon showed the generation of huge hydrostatic pressure in the local area [46]. Such densification behavior induced by hydrostatic stresses was found to be comparable with the behavior of glass under indentation [47]. Consequently, we may consider that the densified layer formed during polishing process is similar to the densified zone created by indentation. Besides, locally enhanced dissolution rates were found at indentation sites on the glass surfaces (silica and floated window glasses) [37]. Therefore, the densified layer formed during glass polishing may contribute to the enhanced short-term alteration rate (**Fig. 5d**). As mentioned above, the indentation-induced densification can be totally cured by the thermal annealing, which is also compatible with the reduction of alteration rates as shown in the short-terme alteration data obtained with annealed glass (**Fig. 5d**).

Underlying the macroscopic densification are the modification in glass structural network. For silicate glasses densified under high pressure or indentation, it has been found the decrease of Si-O-Si angles between silicon tetrahedrons and the increase in Q_2 species (Si-O– stretching in a structural unit with n non-bridging O atoms) at the expense of Q_3 species [48] (Taniguchi 2004). Hence, the decrease in inter-tetrahedral angle could increase effectively the chemical activity of Si-O-Si bonds, resulting in a lower resistance to hydrolysis [49]. These structural changes can be identified by Raman spectroscopy, where the changes in mean angle between silicon tetrahedrons could be characterized by a shift of Raman spectra towards higher frequency at round 500 cm^{-1} [48,50–52]. However, the structural modifications on the annealed samples in this study were not successfully characterized with Raman spectrometry (**Fig. A8** in Supplementary data), which might be due to the relatively thin densified layer in front of the spatial resolution of micro-Raman probe. Besides, the presence of boron in the glass network leads to the mixture of B-O-B, B-O-Si, and Si-O-Si bonds, which makes it more complex for interpreting Raman spectra.

Moreover, the role of boron should not be neglected because the hydration of glass in the vapor phase is always accompanied by boron release. Studies showed that the thermal annealing of the glass may lead to the increase of BO_4 and decrease of non-ring BO_3 in the glass matrix [13,53]. The current work confirms the preferential release of three-coordinated BO_3 in the vapor phase by performing ^{11}B NMR analysis. Recent simulation work on borosilicate glass-water interface showed that BO_3 units are more accessible to water attacks than BO_4 units, which is surrounded by a higher amount of sodium [17]. As a result, the lower release of boron from the annealed glass may be induced by the increase in the fraction of tetrahedral BO_4 whose release may require the prior hydrolysis of the B-O-Si bond.

4.3 Insights into the mechanism of boron release

Considering the possible hydrolysis process during glass vapor hydration, especially the hydrolysis of B-O-Si bonds, linear regressions between chemical thickness (thickness of hydrated layer estimated through boron release) and time (or square root of time) were performed. As shown in **Fig. 11**, the increases of hydrated layer thickness for P-3 samples (VNaI-22 and VNaI-24) are proportional to the square root of time, which suggests a diffusion-controlled process of boron release [10,54]. By applying Fick's second law, the apparent diffusion coefficients for boron were calculated to be $(2.5 \pm 1.2) \times 10^{-20}$ $m^2\ s^{-1}$ for P-3 glass samples. For the P-3-C-A samples (VNaI-31 and VNaI-32), linear increases of hydrated layers can be observed, which implies a hydrolysis-dominating process. As a matter of fact, the constant rate of elemental release has been attributed to the contribution of hydrolysis reaction in the studies of glass aqueous alteration [55]. It is therefore possible that the polishing process has lowered the resistance for the hydrolysis of B-O-Si liaisons in the P-3 glass network, while cured subsequently by thermal annealing in the P-3-A and P-3-C-A glasses. Consequently, the hydrolysis process became a rate-limiting step for the hydration of annealed glass in the vapor phase. The fact that a higher initial aqueous alteration rate is observed with the non-annealed glass samples is compatible with the hypothesis of decrease of B-O-Si hydrolysis barrier, because the hydrolysis process is considered to be a pre-dominant mechanism in controlling the glass initial alteration rate [56,57]. To summarize, the linear regressions performed on the P-3 and P-3-C-A samples suggest the co-presence of diffusion and hydrolysis processes in controlling the release of boron during glass vapor hydration. Noteworthy, between these two processes, the pre-dominant one should depend strongly on the surrounding environment of boron, which consequently controls the kinetics of its release.

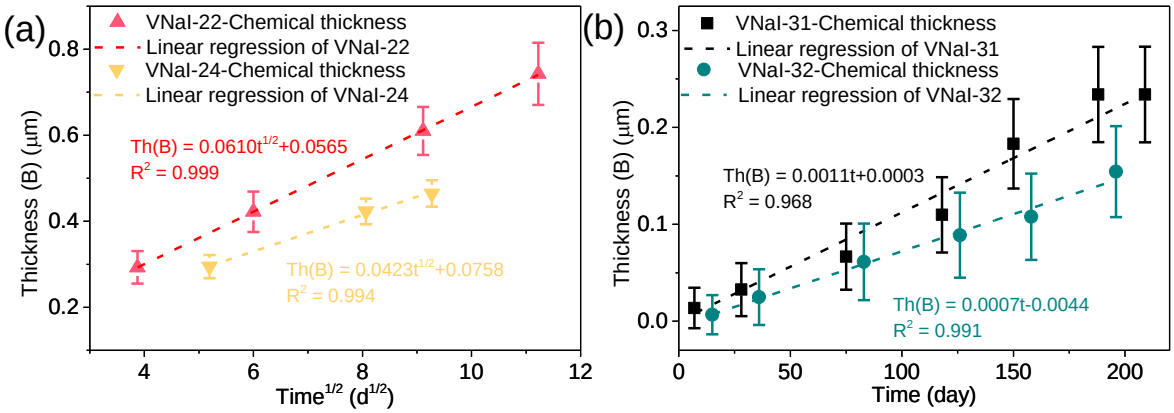

Fig. 11. Linear fitting of chemical thickness: (a) chemical thickness of VNaI-22 and VNaI-24 versus square root of time; (b) chemical thickness of VNaI-31 and VNaI-32 versus time.

Considering the fact that both diffusion and hydrolysis are mechanisms that have been well established to explain the release of elements in the aqueous phase [11,12,25,54,58–62], the proposition of the mechanisms of boron release during glass vapor hydration could be inspired from these existing studies. Recent study on glass aqueous alteration in the silica saturated condition also revealed the important role of boron in controlling the residual rate of glass dissolution [11]. By looking into the experimental observations obtained from the experiments of glass aqueous alteration in the silica-saturated condition and of glass hydration in the unsaturated vapor condition, similarities in boron behaviour could be found. At residual alteration rate, boron (about 12%) and alkali elements (about 25-30%) were found to be retained in the altered gel layer [11,54]. Similar boron and alkali retention ratios were found during the glass vapor hydration [7]. In the silica saturated condition, the release of Si from the glass is largely limited while the release of boron continues [63]. In the unsaturated vapor condition, only the release of boron in the vapor phase was detected. In a study of water adsorption in the unsaturated vapor condition, Asay et al. suggested the presence of three types of water layer structures at relative humidity (RH) higher than 60%: (1) the ice-like layer covering the glass surface, preferably formed by interacting with the silanol groups; (2) a transitional layer that links the ice-like layer and the outmost liquid water layer; (3) the outmost liquid water layer with totally liquid-like configured water layer [64,65]. At 99%RH (the tested experimental condition), tens of monolayers of water molecules could be adsorbed at the surface, including monolayers of liquid-like water [64]. Due to the limited quantity of liquid-like water on the glass surface, the fast increase or even the saturation of boron and silica in the liquid-like water should be expected. Previous study showed that boron could be easily evaporated in the vapor condition [7]. Following the fast increase of boron concentration in the liquid-like water layer, the evaporation of boron could be a rate-limiting factor controlling the rate of glass vapor hydration. Considering the similarity of glass hydration in the vapor phase and glass alteration at residual rate and the previous discussions on the effect annealing, we propose the following mechanisms of glass vapor hydration involving the release of boron:

a) Adsorption of water on the glass surface;

b) Diffusion of water in the glass network and release of Na by inter-diffusion;

c) Proton (occurred after the inter-diffusion and loss of Na^+) catalyses the hydrolysis of B-O-Si bond (which is less resistant than Si-O-Si bond [58]);

d) Diffusion of $BO_{3,\,aq}$ towards the glass surface and accumulation in the liquid-like adsorbed water layer;

e) Evaporation of boron from the liquid-like water layer.

4.4 Transport-limiting property of vapor hydrated layer

It could be implied from the ToF-SIMS profiles of the hydrated glass that the pores in the hydrated layer are mainly formed by the departure of boron and sodium. The release of boron through hydrolysis and diffusion processes results in the formation of silanol groups. The depolymerization of the silicate structure was found in the previous study through Raman analysis [7]. Besides, the degradation of the physical properties in hardness and elastic moduli is coherent with the depolymerization of the glass network. Though the preferential release of boron leads to the increase in the fraction of four-coordinated BO_4 in the hydrated glass, it is not contradictory to the apparent network depolymerization because of the small concentration of boron left in the hydrated layer.

Alteration of the pre-hydrated VNaI glass in DI water shows reduced release of iodine and silicon, which suggests the role of hydrated layer as a blocking barrier. ToF-SIMS characterizations of the hydrated-then-altered layer confirm the accumulation and blockage of boron and iodine at the interface between the pre-hydrated layer and the newly developed altered layer during glass aqueous leaching. During the leaching of the pre-hydrated VNaI glass, the release of boron was not influenced by the presence of the pre-hydrated layer. Besides, the release of boron from the pristine glass and from the hydrated glass are both proportional to the square-root of time, suggesting a diffusion-controlled process. Consequently, the pre-hydrated layer could be considered as a transport-limiting barrier for the release of elements during the subsequent leaching: with the ingress of water molecules through the hydrated layer into the pristine glass, the B-O-Si bonds are hydrolyzed to allow the detachment of boron from the glass network; then the release of the detached boron into the leaching solution is limited by the process of diffusion through the pre-hydrated layer. In terms of iodine retention in the hydrated layer during glass leaching test, aside from the transport-limiting effect, it would be necessary to investigate the structural and chemical environment of iodine, as well as sodium and aluminum which are usually found in the surrounding environment of iodine [66,67].

4.5 Degradation of glass mechanical properties: thickness of the hydrated layer

The decrease of hardness with penetration depth of P-3 sample is well described by the Korsunsky [68] model (**Fig. A9** in Supplementary data) which has proven itself to be well suited for describing the substrate effect on thin film mechanical properties measurements (H, $E_{r,\,sample}$) by instrumented nano indentation. This confirms, if needed, the fact that a thicker softer and certainly more compliant modified layer exists at the outmost surface of P-3 sample as reported in a previous study [69]. Unfortunately, this model with the data in our possession does not allow for the computation of a layer thickness without a proper calibration, which can be done from the thickness (≈ 20 nm) of the hydrated layer provided by the ToF-SIMS technique.

Regarding the VNaI-31 sample for indentation depths ranging from 10 nm to 400 nm, the whole range of possible H and $E_{r,\,sample}$ values (from fully hydrated layer to bulk glass) are covered on the VNaI-31 sample surface (**Fig. 7**). This means that the thickness of the altered layer that has developed at the surface of the sample is highly heterogeneous in thickness. Although the Korsunsky [68] model stands for a homogeneous thin film on a homogeneous substrate geometry, a rough estimation of a possible range of hydrated layer thicknesses is possible. The procedure is explained, and results are presented in Supplementary data (Note 5). As mentioned above, the Korsunsky model is calibrated with P-3 sample, then the model is applied to VNaI-31 data, the film thickness (t) becoming in this case the adjusting parameter. From the $H(h_{max})$ values coming from 16 indentation curves randomly selected in the data set, values of t ranging from 30 to 800 nm are obtained (**Fig. A10** in Supplementary data). The majority of the values lies between 100 and 200 nm (≈50%), the rest is distributed as follow: 20-50 nm (25%), 200-500 (19%), 500-800(8%). The same method was applied to the VNaI-31 homogeneous area, possible values of t were found to range between 600 and 800 nm. It is interesting to note that P-3 H-h_{max} curve (**Fig. 7**) fits almost perfectly the outmost H_{sample} values of VNaI sample, the two having similar hydrated layer thicknesses (20-30 nm range), although their hardness value is different 4.8 GPa for P-3 and 3.2 GPa for VNaI-31. Those values of t compare well with other techniques used in this study in terms of: heterogeneity of the hydrated layer that has developed on VNaI-31 sample; thicknesses of the hydrated layer for P-3 sample but also for VNaI-31 sample for which the 264 nm obtained by FTIR compares relatively well with the values reported above.

5. Conclusion

By studying the mechanical properties and boron release behavior between glass samples possessing different initial states, we propose a mechanism of boron release involving the hydrolysis of B-O-Si bonds followed by the diffusion of three-coordinated boron to the glass/vapor interface. The preferential release of three-coordinated boron is confirmed by ^{11}B NMR analysis. The reduction of glass vapor hydration rate observed for the annealed glass is supposed to be caused by the increase in both the fraction of four-coordinated BO_4 and the energy barrier for B-O-Si hydrolysis. As a result, the surrounding environment of boron in the glass matrix could strongly influence the kinetics of glass vapor hydration. Glass structural modifications indicated by the variations in hardness and elastic modulus bring lights into the understanding of the glass chemical durability, which provides a feasible approach to link the mechanical studies and chemical studies together.

Characterizations of the hydrated glass indicate degradation of the mechanical properties by glass hydration. In the subsequent leaching tests with the hydrated glass sample, the hydrated layer is found to be passivating. The transport-limiting property of the hydrated-layer is verified by the characterizations of the hydrated-then-altered layer. With the tested samples, the initial surface state (including the surface roughness and the surface chemical composition changes induced by annealing) shows negligible effect on the glass vapor hydration. Similarities between glass vapor hydration and glass alteration at residual rate are discussed, which provide insights into further studies to understand the mechanism of glass vapor hydration.

CRediT authorship contribution statement

Haohan Zhang: Conceptualization, Formal analysis, Investigation, Methodology, Writing – original draft, Writing – review & editing. **Jean-Pierre Guin**: Formal analysis, Investigation, Methodology, Funding acquisition, Writing – original draft, Writing – review & editing. **Tomo**

Suzuki-Muresan: Conceptualization, Supervision, Funding acquisition, Writing – review & editing. **Michael Paris**: Methodology, Formal analysis, Validation, Writing – review & editing. **Stéphane Gin**: Conceptualization, Supervision, Resources, Funding acquisition, Writing – review & editing. **Abdesselam Abdelouas**: Conceptualization, Supervision, Funding acquisition, Writing – review & editing.

Declaration of Competing Interest

The authors declare that they have no known competing financial interests or personal relationships that could have appeared to influence the work reported in this paper.

Acknowledgement

This work has been supported in part by the Région Pays de la Loire and the European Union (ERDF), the French Ministry for Higher education, the Brittany region and Rennes Métropole through the CPER Projects PRIN2TAN and GLASS. The authors would like to thank the Pari Scientifique CIPress project which provided technical support to the current study. The authors acknowledge the CEA for providing glass samples. The authors would like to thank Martiane Cabié from Centre Pluridisciplinaire de Microscopie Electronique et de Microanalyse (CP2M) for TEM-EDX analysis. Special thanks to Nicolas Stéphant and Jean-Yves Mevellec from Institut des Matériaux de Nantes (IMN) for SEM analyses and FTIR analysis, respectively. We would like to thank Yann Morizet from Laboratoire de Planétologie et Géodynamique de Nantes (LPGN) for Raman analysis.

References

[1] J. Neeway, A. Abdelouas, B. Grambow, S. Schumacher, C. Martin, M. Kogawa, S. Utsunomiya, S. Gin, P. Frugier, Vapor hydration of SON68 glass from 90 °C to 200 °C: A kinetic study and corrosion products investigation, J. Non. Cryst. Solids. 358 (2012) 2894–2905. https://doi.org/10.1016/j.jnoncrysol.2012.07.020.

[2] A. Ait Chaou, A. Abdelouas, Y. El, C. Martin, A.A. Chaou, A. Abdelouas, Y. El Mendili, R. Bouakkaz, C. Martin, The French SON68 glass vapor hydration under different atmospheres, Procedia Mater. Sci. 7 (2014) 179–185. https://doi.org/http://dx.doi.org/10.1016/j.mspro.2014.10.024.

[3] A. Ait Chaou, A. Abdelouas, Y. El Mendili, R. Bouakkaz, S. Utsunomiya, C. Martin, X. Bourbon, Vapor hydration of a simulated borosilicate nuclear waste glass in unsaturated conditions at 50 °C and 90 °C, RSC Adv. 5 (2015) 64538–64549. https://doi.org/10.1039/c5ra12384d.

[4] A. Ait Chaou, A. Abdelouas, Y. El Mendili, C. Martin, The role of pH in the vapor hydration at 175 °C of the French SON68 glass, Appl. Geochemistry. 76 (2017) 22–35. https://doi.org/10.1016/j.apgeochem.2016.11.006.

[5] S. Narayanasamy, P. Jollivet, N. Godon, F. Angeli, S. Gin, M. Cabié, J. Cambedouzou, C. Le Guillou, A. Abdelouas, Influence of composition of nuclear waste glasses on vapor phase hydration, J. Nucl. Mater. 525 (2019) 53–71. https://doi.org/10.1016/j.jnucmat.2019.07.015.

[6] S. Narayanasamy, P. Jollivet, L. Sessegolo, F. Angeli, A. Abdelouas, Influence of temperature and relative humidity on vapor hydration of an AVM nuclear waste glass, J. Nucl. Mater. 543 (2021) 152571. https://doi.org/10.1016/j.jnucmat.2020.152571.

[7] H. Zhang, T. Suzuki-Muresan, Y. Morizet, S. Gin, A. Abdelouas, Investigation on boron and iodine behavior during nuclear glass vapor hydration, Npj Mater. Degrad. 5 (2021) 10. https://doi.org/10.1038/s41529-021-00157-6.

[8] C. Jegou, S. Narayanasamy, F. Angeli, Short communication on the Influence of the temperature between 30 and 70°C on the hydration of SON68 nuclear waste glass in a vapour phase, J. Nucl. Mater. 545 (2021) 152738. https://doi.org/10.1016/j.jnucmat.2020.152738.

[9] R. Bouakkaz, Altération aqueuse et hydratation en phase vapeur duverre SON68 à basse température (35-90 ° C), Ecole des Mines de Nantes, 2014.

[10] P. Frugier, S. Gin, Y. Minet, T. Chave, B. Bonin, N. Godon, J.E. Lartigue, P. Jollivet, A. Ayral, L. De Windt, G. Santarini, SON68 nuclear glass dissolution kinetics: Current state of knowledge and basis of the new GRAAL model, J. Nucl. Mater. 380 (2008) 8–21. https://doi.org/10.1016/j.jnucmat.2008.06.044.

[11] S. Gin, X. Guo, J.M. Delaye, F. Angeli, K. Damodaran, V. Testud, J. Du, S. Kerisit, S.H. Kim, Insights into the mechanisms controlling the residual corrosion rate of borosilicate glasses, Npj Mater. Degrad. 4 (2020) 41. https://doi.org/10.1038/s41529-020-00145-2.

[12] M. Collin, M. Fournier, P. Frugier, T. Charpentier, M. Moskura, L. Deng, M. Ren, J. Du, S. Gin, Structure of International Simple Glass and properties of passivating layer formed in circumneutral pH conditions, Npj Mater. Degrad. 2 (2018) 4. https://doi.org/10.1038/s41529-017-0025-y.

[13] F. Angeli, T. Charpentier, P. Jollivet, D. de Ligny, M. Bergler, A. Veber, S. Gin, H. Li, Effect of thermally induced structural disorder on the chemical durability of International Simple Glass, Npj Mater. Degrad. 2 (2018). https://doi.org/10.1038/s41529-018-0052-3.

[14] G. Geneste, F. Bouyer, S. Gin, Hydrogen-sodium interdiffusion in borosilicate glasses investigated from first principles, J. Non. Cryst. Solids. 352 (2006) 3147–3152. https://doi.org/10.1016/j.jnoncrysol.2006.04.023.

[15] H. Aréna, R. Podor, H.P. Brau, J. Nelayah, N. Godon, M. Cabié, E. Garcès, C. Mansas, D. Rébiscoul, Characterization of the boron profile and coordination in altered glass layers by EEL spectroscopy, Micron. 141 (2021). https://doi.org/10.1016/j.micron.2020.102983.

[16] P. Zapol, H. He, K.D. Kwon, L.J. Criscenti, First-principles study of hydrolysis reaction barriers in a sodium borosilicate glass, Int. J. Appl. Glas. Sci. 4 (2013) 395–407. https://doi.org/10.1111/ijag.12052.

[17] H. Jabraoui, T. Charpentier, S. Gin, J.-M. Delaye, R. Pollet, Atomic Insights into the Events Governing the Borosilicate Glass–Water Interface, J. Phys. Chem. C. 125 (2021) 7919–7931. https://doi.org/10.1021/acs.jpcc.1c00388.

[18] D. Nečas, P. Klapetek, Gwyddion: an open-source software for SPM data analysis, Open Phys. 10 (2012) 181–188. https://doi.org/doi:10.2478/s11534-011-0096-2.

[19] W.C. Oliver, G.M. Pharr, An improved technique for determining hardness and elastic modulus using load and displacement sensing indentation experiments, J. Mater. Res. 7 (1992) 1564–1583. https://doi.org/10.1557/jmr.1992.1564.

[20] F. Angeli, T. Charpentier, D. De Ligny, C. Cailleteau, Boron speciation in soda-lime borosilicate glasses containing zirconium, J. Am. Ceram. Soc. 93 (2010) 2693–2704. https://doi.org/10.1111/j.1551-2916.2010.03771.x.

[21] V. Jolivet, L. Jossé, M. Rivoal, M. Paris, Y. Morizet, L. Carole, T. Suzuki-Muresan, Quantification of boron in aluminoborosilicate glasses using Raman and 11 B NMR, J. Non. Cryst. Solids. 511 (2019) 50–61. https://doi.org/10.1016/j.jnoncrysol.2018.12.038.

[22] D. Massiot, F. Fayon, M. Capron, I. King, S. Le Calvé, B. Alonso, J.O. Durand, B. Bujoli, Z. Gan, G. Hoatson, Modelling one- and two-dimensional solid-state NMR spectra, Magn. Reson. Chem. 40 (2002) 70–76. https://doi.org/10.1002/mrc.984.

[23] T. Suratwala, W. Steele, L. Wong, M.D. Feit, P.E. Miller, R. Dylla-Spears, N. Shen, R. Desjardin, Chemistry and Formation of the Beilby Layer during Polishing of Fused Silica Glass, J. Am. Ceram. Soc. 98 (2015) 2395–2402. https://doi.org/10.1111/jace.13659.

[24] M. Py, Study of interfaces and nanometric structures by ToF-SIMS : upon a spatially resolved quantitative analysis, Université de Grenoble, 2011.

[25] S. Gin, M. Collin, P. Jollivet, M. Fournier, Y. Minet, L. Dupuy, T. Mahadevan, S. Kerisit, J. Du, Dynamics of self-reorganization explains passivation of silicate glasses, Nat. Commun. 9 (2018) 1–9. https://doi.org/10.1038/s41467-018-04511-2.

[26] F. Angeli, M. Gaillard, P. Jollivet, T. Charpentier, Influence of glass composition and alteration solution on leached silicate glass structure: A solid-state NMR investigation, Geochim. Cosmochim. Acta. 70 (2006) 2577–2590. https://doi.org/10.1016/j.gca.2006.02.023.

[27] T. Ohkubo, Y. Iwadate, K. Deguchi, S. Ohki, T. Shimizu, Changes in surface structure of sodium aluminoborosilicate glasses during aqueous corrosion analyzed by using NMR, J. Phys. Chem. Solids. 77 (2015) 164–171. https://doi.org/10.1016/j.jpcs.2014.10.018.

[28] W.J. Dell, P.J. Bray, S.Z. Xiao, 11B NMR studies and structural modeling of Na2OB2O3SiO2 glasses of high soda content, J. Non. Cryst. Solids. 58 (1983) 1–16. https://doi.org/10.1016/0022-3093(83)90097-2.

[29] L.S. Du, J.F. Stebbins, Nature of silicon-boron mixing in sodium borosilicate glasses: A high-resolution 11B and 17O NMR study, J. Phys. Chem. B. 107 (2003) 10063–10076. https://doi.org/10.1021/jp034048l.

[30] F.W. Preston, The structure of abraded glass surfaces, Trans. Opt. Soc. 23 (1922) 141. https://doi.org/10.1088/1475-4878/23/3/301.

[31] Beilby G. T., Surface flow in crystalline solids under mechanical disturbance, Proc. R. Soc. London. 72 (1904) 218–225. https://doi.org/10.1098/rspl.1903.0045.

[32] L. Névot, P. Croce, Caractérisation des surfaces par réflexion rasante de rayons X. Application à l'étude du polissage de quelques verres silicates, Rev. Phys. Appliquée. 15 (1980) 761–779. https://doi.org/10.1051/rphysap:01980001503076100.

[33] J.A. Trogolo, K. Rajan, Near surface modification of silica structure induced by chemical/mechanical polishing, J. Mater. Sci. 1994 2917. 29 (2004) 4554–4558. https://doi.org/10.1007/BF00376278.

[34] W. Bensch, W. Bergholz, An FT-IR study of silicon dioxides for VLSI microelectronics, Semicon Sci. Tech. 5 (1990) 421. https://doi.org/10.1088/0268-1242/5/5/008.

[35] S. Yoshida, J.-C. Sanglebœuf, T. Rouxel, Quantitative evaluation of indentation-induced densification in glass, J. Mater. Res. 20 (2005) 3404–3412. https://doi.org/10.1557/jmr.2005.0418.

[36] J.D. MACKENZIE, High-Pressure Effects on Oxide Glasses: II, Subsequent Heat Treatment, J. Am. Ceram. Soc. 46 (1963) 470–476. https://doi.org/10.1111/J.1151-2916.1963.TB13777.X.

[37] Y.-F. Niu, K. Han, J.-P. Guin, Locally Enhanced Dissolution Rate as a Probe for Nanocontact-Induced Densification in Oxide Glasses, Langmuir. 28 (2012) 10733–10740. https://doi.org/10.1021/la300972j.

[38] L.T. Zhuravlev, The surface chemistry of amorphous silica. Zhuravlev model, Colloids Surfaces A Physicochem. Eng. Asp. 173 (2000) 1–38. https://doi.org/10.1016/S0927-7757(00)00556-2.

[39] H. Liu, D. Ngo, M. Ren, J. Du, S.H. Kim, Effects of surface initial condition on aqueous corrosion of glass—A study with a model nuclear waste glass, J. Am. Ceram. Soc. 102 (2019) 1652–1664. https://doi.org/10.1111/jace.16016.

[40] J. Banerjee, V. Bojan, C.G. Pantano, S.H. Kim, Effect of heat treatment on the surface chemical structure of glass: Oxygen speciation from in situ XPS analysis, J. Am. Ceram. Soc. 101 (2018) 644–656. https://doi.org/10.1111/JACE.15245.

[41] D.R. Tadjiev, R.J. Hand, P. Zeng, Comparison of glass hydration layer thickness measured by transmission electron microscopy and nanoindentation, Mater. Lett. 64 (2010) 1041–1044. https://doi.org/10.1016/J.MATLET.2010.02.004.

[42] W. -T Han, M. Tomozawa, Indentation Creep of Na2O · 3SiO2 Glasses with Various Water Contents, J. Am. Ceram. Soc. 73 (1990) 3626–3632. https://doi.org/10.1111/J.1151-2916.1990.TB04268.X.

[43] N.M. Keulen, Indentation Creep of Hydrated Soda–Lime Silicate Glass Determined by Nanoindentation, J. Am. Ceram. Soc. 76 (1993) 904–912. https://doi.org/10.1111/J.1151-2916.1993.TB05314.X.

[44] J.A. Trogolo, K. Rajan, Near surface modification of silica structure induced by chemical/mechanical polishing, J. Mater. Sci. 29 (1994) 4554–4558. https://doi.org/10.1007/BF00376278.

[45] J.C. Lambropoulos, S. Xu, T. Fang, Constitutive law for the densification of fused silica, with applications in polishing and microgrinding, J. Am. Ceram. Soc. 79 (1996) 1441–1452. https://doi.org/10.1111/j.1151-2916.1996.tb08748.x.

[46] X. Han, Y. Hu, S. Yu, Investigation of material removal mechanism of silicon wafer in the chemical mechanical polishing process using molecular dynamics simulation method, Appl. Phys. A Mater. Sci. Process. 95 (2009) 899–905. https://doi.org/10.1007/s00339-009-5097-2.

[47] H. Ji, V. Keryvin, T. Rouxel, T. Hammouda, Densification of window glass under very high pressure and its relevance to Vickers indentation, Scr. Mater. 55 (2006) 1159–1162. https://doi.org/10.1016/j.scriptamat.2006.08.038.

[48] T. Deschamps, C. Martinet, J.L. Bruneel, B. Champagnon, Soda-lime silicate glass under hydrostatic pressure and indentation: a micro-Raman study, J. Phys. Condens. Matter. 23 (2011) 035402. https://doi.org/10.1088/0953-8984/23/3/035402.

[49] T.A. Michalske, B.C. Bunker, Slow fracture model based on strained silicate structures, J. Appl. Phys. 56 (1984) 2686–2693. https://doi.org/10.1063/1.333789.

[50] A. Winterstein-Beckmann, D. Möncke, D. Palles, E.I. Kamitsos, L. Wondraczek, A Raman-spectroscopic study of indentation-induced structural changes in technical alkali-borosilicate glasses with varying silicate network connectivity, J. Non. Cryst. Solids. 405 (2014) 196–206. https://doi.org/10.1016/j.jnoncrysol.2014.09.020.

[51] S. Peuget, J.M. Delaye, C. Jégou, Specific outcomes of the research on the radiation stability of the French nuclear glass towards alpha decay accumulation, J. Nucl. Mater. 444 (2014) 76–91. https://doi.org/10.1016/j.jnucmat.2013.09.039.

[52] D. Vandembroucq, T. Deschamps, C. Coussa, A. Perriot, E. Barthel, B. Champagnon, C. Martinet, Density hardening plasticity and mechanical ageing of silica glass under pressure: a Raman spectroscopic study, J. Phys. Condens. Matter. 20 (2008) 485221. https://doi.org/10.1088/0953-8984/20/48/485221.

[53] N. Stone-Weiss, E.M. Pierce, R.E. Youngman, O. Gulbiten, N.J. Smith, J. Du, A. Goel, Understanding the structural drivers governing glass–water interactions in borosilicate based model bioactive glasses, Acta Biomater. 65 (2018) 436–449. https://doi.org/10.1016/j.actbio.2017.11.006.

[54] P. Frugier, S. Gin, J.E. Lartigue, E. Deloule, SON68 glass dissolution kinetics at high reaction progress: Mechanisms accounting for the residual alteration rate, Mater. Res. Soc. Symp. Proc. 932 (2006) 305–312.

[55] M.I. Ojovan, R.J. Hand, N. V. Ojovan, W.E. Lee, Corrosion of alkali-borosilicate waste glass K-26 in non-saturated conditions, J. Nucl. Mater. 340 (2005) 12–24. https://doi.org/10.1016/j.jnucmat.2004.10.095.

[56] J.D. Vienna, J. V. Ryan, S. Gin, Y. Inagaki, Current understanding and remaining challenges in modeling long-term degradation of borosilicate nuclear waste glasses, Int. J. Appl. Glas. Sci. 4 (2013) 283–294. https://doi.org/10.1111/ijag.12050.

[57] S. Gin, J.-M. Delaye, F. Angeli, S. Schuller, Aqueous alteration of silicate glass: state of knowledge and perspectives, Npj Mater. Degrad. 5 (2021) 42. https://doi.org/10.1038/s41529-021-00190-5.

[58] B.C. Bunker, G.W. Arnold, D.E. Day, P.J. Bray, The effect of molecular structure on borosilicate glass leaching, J. Non. Cryst. Solids. 87 (1986) 226–253. https://doi.org/10.1016/S0022-3093(86)80080-1.

[59] B.C. Bunker, Molecular mechanisms for corrosion of silica and silicate glasses, J. Non. Cryst. Solids. 179 (1994) 300–308. https://doi.org/10.1016/0022-3093(94)90708-0.

[60] S. Gin, P. Jollivet, G. Barba Rossa, M. Tribet, S. Mougnaud, M. Collin, M. Fournier, E. Cadel, M. Cabie, L. Dupuy, Atom-Probe Tomography, TEM and ToF-SIMS study of borosilicate glass alteration rim: A multiscale approach to investigating rate-limiting mechanisms, Geochim. Cosmochim. Acta. 202 (2017) 57–76. https://doi.org/10.1016/j.gca.2016.12.029.

[61] P. Frugier, T. Chave, S. Gin, J.E. Lartigue, Application of the GRAAL model to leaching experiments with SON68 nuclear glass in initially pure water, J. Nucl. Mater.

392 (2009) 552–567.
http://www.sciencedirect.com/science/article/pii/S0022311509005996.

[62] S. Gin, A.H. Mir, A. Jan, J.M. Delaye, E. Chauvet, Y. De Puydt, A. Gourgiotis, S. Kerisit, A General Mechanism for Gel Layer Formation on Borosilicate Glass under Aqueous Corrosion, J. Phys. Chem. C. 124 (2020) 5132–5144. https://doi.org/10.1021/acs.jpcc.9b10491.

[63] J. Neeway, A. Abdelouas, B. Grambow, S. Schumacher, Dissolution mechanism of the SON68 reference nuclear waste glass: New data in dynamic system in silica saturation conditions, J. Nucl. Mater. 415 (2011) 31–37. https://doi.org/10.1016/j.jnucmat.2011.05.027.

[64] D.B. Asay, S.H. Kim, Evolution of the adsorbed water layer structure on silicon oxide at room temperature, J. Phys. Chem. B. 109 (2005) 16760–16763. https://doi.org/10.1021/jp053042o.

[65] D.B. Asay, A.L. Barnette, S.H. Kim, Effects of surface chemistry on structure and thermodynamics of water layers at solid-vapor interfaces, J. Phys. Chem. C. 113 (2009) 2128–2133. https://doi.org/10.1021/jp806815p.

[66] B.J. Riley, M.J. Schweiger, D.S. Kim, W.W. Lukens, B.D. Williams, C. Iovin, C.P. Rodriguez, N.R. Overman, M.E. Bowden, D.R. Dixon, J. V. Crum, J.S. McCloy, A.A. Kruger, Iodine solubility in a low-activity waste borosilicate glass at 1000 °c, J. Nucl. Mater. 452 (2014) 178–188. https://doi.org/10.1016/j.jnucmat.2014.04.027.

[67] D.A. McKeown, I.S. Muller, I.L. Pegg, Iodine valence and local environments in borosilicate waste glasses using X-ray absorption spectroscopy, J. Nucl. Mater. 456 (2015) 182–191. https://doi.org/10.1016/j.jnucmat.2014.09.033.

[68] A.M. Korsunsky, M.R. McGurk, S.J. Bull, T.F. Page, On the hardness of coated systems, Surf. Coatings Technol. 99 (1998) 171–183. https://doi.org/10.1016/S0257-8972(97)00522-7.

[69] B.L. Hackett, A.A. Wereszczak, G.M. Pharr, Effect of aqueous-based mechanical polishing on the nanoindentation response of borosilicate glasses, Int. J. Appl. Glas. Sci. 10 (2019) 302–306. https://doi.org/10.1111/IJAG.13108.